A Pressure-Based Model for Two-Phase Flows Under Generic Equations of State

Barbara Re[1(✉)], Giuseppe Sirianni[1], and Rémi Abgrall[2]

[1] Department of Aerospace, Science and Technology, Politecnico di Milano, Milano, Italy
{barbara.re,giuseppe.sirianni}@polimi.it
[2] Institute of Mathematics, University of Zurich, Zurich, Switzerland
remi.abgrall@math.uzh.ch

Abstract. We present a diffuse interface method for a pressure-based Baer-Nunziato type model for compressible two-phase flows, which allows the use of generic equations of state to describe each phase. The model is made dimensionless by means of a special pressure scaling that recovers the correct scaling of the discrete governing equations in the zero Mach limit, and overcomes the difficulties related to the lack of a clear notion of reference speed of sound in non-equilibrium two-phase flows. The model is equipped with pressure and velocity relaxation terms to impose the mechanical equilibrium between phases after their independent evolution. Two different finite volume schemes are presented. First, a 1D semi-implicit staggered scheme is introduced to show the capability of the model to work with the Peng-Robinson EOS when each phase evolves close to the saturation curve. Then, a preliminary 2D explicit scheme, which does not include the relaxation terms, is presented as a first step toward the development of an unstructured 2D scheme for compressible two-phase flows at all Mach numbers. The validity of the preliminary 2D monolithic implementation of the hyperbolic operator is illustrated through the simulation of a shock-bubble interaction with air and helium.

Keywords: compressible two-phase flows · Baer-Nunziato model · low Mach · finite volume scheme

1 Introduction

Compressible two-phase flows occur in NICFD regimes, especially in applications involving organic fluids and CO_2 flows. An example is represented by Organic Rankine cycles (ORCs) operating with the so-called wet-to-dry expansion allowed by the high molecular complexity of the working fluids, which may result in a positive slope of the vapor-liquid equilibrium (VLE) curve in the temperature–entropy (T–s) plane. The two-phase expansion could considerably increase the power performance of waste heat recovery systems [15]. Another

M. White et al. (Eds.): NICFD 2022, ERCOFTAC 29, pp. 146–155, 2023.
https://doi.org/10.1007/978-3-031-30936-6_15

example is the transportation of dense CO_2 through pressurized pipelines along the Carbon Capture and Storage (CCS) chain, where a harmful pipeline failure likely results in two-phase flows [4]. To investigate the flow behavior in these and similar conditions, simulation tools able to model two-phase flows in NICFD regimes are mandatory.

Diffuse-interface methods (DIMs) are efficient strategies to model unsteady compressible multi-component or multi-phase flows, consisting of two or more immiscible fluids or components, that exhibit some level of separation at a scale above the molecular level [12]. DIMs do not describe a local instantaneous realization of the flow, but its behavior on average, so they are well suited to dispersed flows, e.g., droplets dispersed in a continuous carrier phase, but they are flexible enough to describe almost pure fluids as well. These methods rely on augmented systems of governing equations that specifically model the behavior of the continuum close to the interfaces, whereas they recover the pure fluid behavior in the bulk. The dynamic interfaces separating different fluids or components are not explicitly tracked, but they are reconstructed from an indicator function.

The cornerstone of the DIM class is the Baer and Nunziato (BN) model, which assumes that each component evolves with its own pressure, temperature, and density. Hence, each component is treated as a separate continuum with its own thermodynamic model. This last feature is of paramount importance to be able to select the proper equation of state (EOS) to describe the thermodynamic behavior in the NICFD regime.

From the full non-equilibrium models, reduced models are derived assuming the equilibrium between one or more variables, e.g. the five-equation model by Kapila assumes mechanical equilibrium among phases, which evolve with the same pressure and velocity. This assumption simplifies the model, reducing the number of governing equations, but introduces serious computational challenges, such as the non-conservative term in the equation for the volume fraction that depends on the divergence of the velocity, and the non-monotone behavior of the sound speed to the volume fraction [13]. Furthermore, modeling important phenomena such phase slip and non-equilibrium liquid/vapor transition is important, especially in two-phase flow applications involving dense gases that undergo mass transfer [3].

We consider a recent pressure-based BN-type model [9] able to deal with generic EOSs and equipped with relaxation parameters, which can be used to control whether the phasic pressure and/or velocity are driven toward the equilibrium. In this work, we show its capability to work with different EOSs, and we present the preliminary results in 2D.

2 The Model

The pressure-based BN-type model developed by Re and Abgrall [9] reads

$$\frac{\partial \alpha_i}{\partial t} = -\mathbf{u}_{\mathrm{IN}} \cdot \boldsymbol{\nabla}\alpha_i + \mu \Delta_i P \tag{1a}$$

$$\frac{\partial (\alpha_i \rho_i)}{\partial t} + \boldsymbol{\nabla} \cdot (\alpha_i \rho_i \mathbf{u}_i) = 0 \tag{1b}$$

$$\frac{\partial (\alpha_i \rho_i \mathbf{u}_i)}{\partial t} + \boldsymbol{\nabla} \cdot (\alpha_i \rho_i \mathbf{u}_i \otimes \mathbf{u}_i + \alpha_i P_i \mathbb{I}) = P_{\mathrm{IN}} \boldsymbol{\nabla}\alpha_i - \lambda \Delta_i \mathbf{u} \tag{1c}$$

$$\begin{aligned} M_{\mathrm{ref}}^2 \left[\alpha_i \frac{\partial P_i}{\partial t} + \alpha_i \mathbf{u}_i \cdot (\boldsymbol{\nabla} P_i) + (\alpha_i \rho_i c_i^2) \boldsymbol{\nabla} \cdot \mathbf{u}_i \right] &= \kappa_i \left[\mathbf{u}_{\mathrm{IN}} \cdot \boldsymbol{\nabla}\alpha_i - \mu \Delta_i P - \boldsymbol{\nabla} \cdot (\alpha_i \mathbf{u}_i) \right] \\ &+ M_{\mathrm{ref}}^2 \Big[\rho_i c_{i,\mathrm{IN}}^2 \left[(\mathbf{u}_{\mathrm{IN}} - \mathbf{u}_i) \cdot \boldsymbol{\nabla}\alpha_i - \mu \Delta_i P \right] \\ &- \kappa_i \lambda (\mathbf{u}_{\mathrm{IN}} - \mathbf{u}_i) \cdot \Delta_i \mathbf{u} \Big] \end{aligned} \tag{1d}$$

where the subscript $i = \{1, 2\}$ indicates the phase, α the volume fraction, ρ the density, $\mathbf{u}$ the velocity, P the pressure, c the speed of sound, μ and λ are relaxation parameters which can be used to reproduce different multi-phase flow topologies. For instance, λ can be defined in terms of the specific interfacial area and the acoustic impedances of the fluids [12], whereas μ is an homogenization parameter whose physical meaning has been justified with considerations based on the second law of thermodynamics by Baer and Nunziato [2]. The operator Δ_i expresses the signed jump in a variable between phases, e.g., $\Delta_1 \mathbf{u} = \mathbf{u}_1 - \mathbf{u}_2$. The subscript IN indicates interfacial quantities: $\mathbf{u}_{\mathrm{IN}}$ and P_{IN} are closure terms and they are defined as weighted averages

$$\mathbf{u}_{\mathrm{IN}} = \frac{\alpha_1 \rho_1 \mathbf{u}_1 + \alpha_2 \rho_2 \mathbf{u}_2}{\alpha_1 \rho_1 + \alpha_1 \rho_1} \qquad \text{and} \qquad P_{\mathrm{IN}} = \alpha_1 P_1 + \alpha_2 P_2 \,, \tag{2}$$

whereas $c_{i,\mathrm{IN}}$ is the intefacial speed of sound, which does not have any thermodynamic meaning but it is defined by analogy with the speed of sound:

$$c_i^2 = \chi_i + \kappa_i \frac{P_i + e_i}{\rho_i} \quad \text{and} \quad c_{i,\mathrm{IN}}^2 = \chi_i + \kappa_i \frac{P_{\mathrm{IN}} + e_i}{\rho_i}, \qquad \text{with} \quad \kappa = \left(\frac{\partial P}{\partial e} \right)_\rho \quad \text{and} \quad \chi = \left(\frac{\partial P}{\partial \rho} \right)_e , \tag{3}$$

where e is the internal energy per unit of volume. Equations (1b)–(1d) are repeated for both phases, while Eq. (1a) is solved only for phase 1, as the constraint $\alpha_1 + \alpha_2 = 1$ holds. Thanks to the symmetry of the model, which phase is solved as 1 does not affect the results.

2.1 The Low-Mach Scaling

The system of Eqs. (1) is dimensionless and it includes a special pressure scaling, according to which the dimensionless pressure P is defined as $P = \left(\tilde{P} - \tilde{P}_{\mathrm{ref}} \right) / \tilde{\rho}_{\mathrm{ref}} \tilde{u}_{\mathrm{ref}}^2$, where $\sim$ indicates a dimensional quantity, and the subscript "ref" a reference quantity. In addition, a reference Mach number M_{ref} is defined as $M_{\mathrm{ref}}^2 = \tilde{\rho}_{\mathrm{ref}} \tilde{u}_{\mathrm{ref}}^2 / \tilde{P}_{\mathrm{ref}}$, which expresses the global level of compressibility of the flow field. This peculiar scaling overcomes the singularity in the

limit $M \to 0$ that affects standard compressible schemes that assume a non-dimensional scaling based on a single reference velocity, for instance a reference speed of sound, which results in the term $1/M^2$ in front of the pressure gradient in the momentum equation. In this context, we remark that for non-equilibrium two-phase flows, there is not a clear notion of mixture speed of sound, so the choice of a reference speed of sound is ambiguous, if not impossible. Moreover, the adopted scaling allows the recovery of the correct limit of the governing equations in the incompressible regime [9].

2.2 Thermodynamic Model

The model of Eqs. (1) assumes a generic description of the thermodynamics of each fluid, with the only requirement to express the pressure EOS as $e = e(\rho, P)$. Most of the EOSs used for academic and industrial purposes, especially cubic ones, can easily meet this requirement, so they can model the thermodynamic behavior of each component. Moreover, different EOSs can be adopted for different phases.

Particular attention should be paid while scaling the thermodynamic definition involving the pressure, as they can involve the additional term $\tilde{P}_{\text{ref}}$. For instance, the relation between the dimensional and dimensionless speed of sound reads

$$\tilde{c}^2 = \tilde{\chi} + \tilde{\kappa}\frac{\tilde{P} + \tilde{e}}{\tilde{\rho}} = \left[\chi + \kappa\frac{P + e}{\rho}\right]\tilde{u}_{\text{ref}}^2 + \frac{\kappa}{\rho}\frac{\tilde{P}_{\text{ref}}}{\tilde{\rho}_{\text{ref}}} = \left[c^2 + \frac{\kappa}{\rho M_{\text{ref}}^2}\right]\tilde{u}_{\text{ref}}^2 . \tag{4}$$

In this work, we consider two different EOSs: the stiffened gas model and the Peng-Robinson EOS. Considering the former, it is possible to directly define the dimensionless definitions according to the special low Mach scaling described in the previous subsection. The pressure EOS is defined as

$$P(e, \rho) = (\gamma - 1)e - \gamma P_\infty - (\gamma - 1)\rho q - 1/M_{\text{ref}}^2 , \tag{5}$$

where γ, P_∞, and q are substance-specific parameters [7]. The compatible caloric EOS, derived under the polytropic assumption following [10] is

$$e(T, \rho) = c_v \rho T + \rho q + P_\infty \qquad \text{or} \qquad P(T, \rho) = (\gamma - 1)c_v \rho T - P_\infty - \frac{1}{M_{\text{ref}}^2} , \tag{6}$$

where T is the temperature, and c_v is the isochoric specific heat.

Concerning the Peng-Robinson EOS, we use an external thermodynamic library developed at SINTEF (Norway), which exploits the concept of the corresponding states to enhance the accuracy of specific properties, such as the density and the speed of sound, computed through the Peng-Robinson EOS for the liquid phase [16]. Then, the results of the library are made dimensionless, according to the special scaling described above, e.g. in Sec. 2.1 and Eq. (4).

3 Numerical Method

The solution strategy for the system of Eqs. (1) is here briefly summarized. A detailed description for the 1D can be found in [9]. The Strang splitting approach is used to solve the system of partial differential equations (PDEs): at each time step, two operators are consecutively applied. First, the hyperbolic operator solves the PDEs composed without the relaxation terms, then the relaxation operator solves the system of ordinary differential equations (ODEs) composed only by the temporal derivatives and the relaxation terms.

3.1 Hyperbolic Operator in 1D: A Semi-implicit Staggered Scheme

A semi-implicit time integration scheme is used to reach an acceptable computational efficiency without running into a too severe restriction on the time step. The acoustic terms, generally linear, are integrated implicitly in time, while the convective terms are integrated explicitly. In this way, the stability constraint on the time step is based only on the convective velocity, but the non-linearity of the system is weaker than the full implicit time integration.

The pressure-based formulation of the BN-type model is solved through a segregate solution approach, according to which, at each time step, the momenta (or the velocities) are first predicted considering the pressures at the previous time step, then, the new pressures are computed, and, finally, the momenta are updated for the pressure correction.

A finite volume scheme is used to spatially discretize the governing equations. A staggered grid is used to combine different discretizations. For simplicity, the convective terms are approximated using first-order Rusanov fluxes, which circumvent the need to solve a Riemann problem at cell interfaces. A central finite difference approximation is adopted for the gradient of the pressure in Eq. (1c) and the divergence of the velocity in Eq. (1d). A robust discretization of the non-conservative terms involving the gradient of the volume fraction is derived following the non-disturbance conditions, which states that a flow uniform in pressure and velocity should remain uniform in these variables at the next time steps [1].

3.2 Source Operator

Velocity and pressure relaxation give rise to two ODE problems, which include only time derivatives and the right-hand side terms of Eqs. (1) involving λ and μ. These systems are solved sequentially: first, the solution computed by the hyperbolic operator (labeled $\mathrm{L_{hyp}}$) is evolved towards the velocity equilibrium by the operator $\mathrm{R_{vel}}$; then, this result is used as initial condition for $\mathrm{R_{pres}}$ to relax the pressures. The solution strategy at each time step can be summarized as:

$$\mathbf{U}^{n+1} = \mathrm{R_{pres}}\left(\mathbf{U}^{\diamond}\right) \longleftarrow \mathbf{U}^{\diamond} = \mathrm{R_{vel}}\left(\mathbf{U}^{\triangleright}\right) \longleftarrow \mathbf{U}^{\triangleright} = \mathrm{L_{hyp}}\left(\mathbf{U}^{n}\right), \tag{7}$$

where the subscripts $\triangleright$ and $\diamond$ indicate intermediate solution between the time step t^n and t^{n+1}.

We impose instantaneous relaxation, e.g., we consider λ and μ as infinite. As explained in [8], the results of $\mathrm{R_{vel}}$ are

$$\alpha_i^\diamond = \alpha_i^\triangleright, \qquad \rho_i^\diamond = \rho_i^\triangleright, \qquad \mathbf{u}^\diamond = \mathbf{u}_1^\diamond = \mathbf{u}_2^\diamond = \frac{\alpha\rho\mathbf{u}_1^\triangleright + \alpha\rho\mathbf{u}_2^\triangleright}{\alpha\rho_1^\triangleright + \alpha\rho_2^\triangleright}, \qquad \text{and}$$
$$P_i^\diamond = P_i^\triangleright - \rho_i \frac{\kappa_i}{2} \left(\mathbf{u}_{\mathrm{IN}}^\triangleright - \mathbf{u}_i^\triangleright\right) \cdot \left(\mathbf{u}^\diamond - \mathbf{u}_i^\triangleright\right) .$$

The ODE problem for the pressure relaxation includes an equation for α_1, deriving from Eq. (1a), and one equation for each pressure, coming from Eq. (1d). We integrate it using a backward Euler scheme, but we introduce in the definition of the interface speed of sound $c^2_{\mathrm{IN},i}$ suitable approximations $\overline{P_{\mathrm{IN},i}}$ and $\overline{e_i}$ (defined in Algorithm 1), which are kept constant during time integration to mitigate its non-linearity [11]. The discrete equations for the pressures read

$$f_P(P_i, \alpha_i) = M_\mathrm{r}^2 \left(P_i - P_i^\diamond\right) - M_\mathrm{r}^2 \chi_i (\alpha\rho_i)^\diamond \left(\frac{1}{\alpha_i} - \frac{1}{\alpha_i^\diamond}\right) + \left[M_\mathrm{r}^2 \kappa_i \left(\overline{P_{\mathrm{IN},i}} + \overline{e}_i\right) + \kappa_i\right] \log\left(\frac{\alpha_i}{\alpha_i^\diamond}\right) = 0. \tag{8}$$

Combining these expressions and imposing pressure equilibrium, we obtain the following non-linear function

$$\begin{aligned} f_\alpha(\alpha_1) = P_1^{n+1} - P_2^{n+1} = M_\mathrm{r}^2 \Bigg[\left(P_1^\diamond - P_2^\diamond\right) + \chi_1 \left(\frac{(\alpha\rho_1)^\diamond}{\alpha_1} - \frac{(\alpha\rho_1)^\diamond}{\alpha_1^\diamond}\right) - \chi_2 \left(\frac{(\alpha\rho_2)^\diamond}{1-\alpha_1} - \frac{(\alpha\rho_2)^\diamond}{\alpha_2^\diamond}\right) \Bigg] \\ - \left[M_\mathrm{r}^2 \kappa_1 \left(\overline{P_{\mathrm{IN},1}} + \overline{e}_1\right) + \kappa_1\right] \log\left(\frac{\alpha_1}{\alpha_1^\diamond}\right) + \left[M_\mathrm{r}^2 \kappa_2 \left(\overline{P_{\mathrm{IN},2}} + \overline{e}_2\right) + \kappa_2\right] \\ \times \log\left(\frac{1-\alpha_1}{\alpha_2^\diamond}\right) = 0 , \end{aligned} \tag{9}$$

where the only unknown is α_1. We solve this equation iteratively, performing at each iteration k, one iteration of Newton's method, but with a convergence criterion based on the pressure difference, as illustrated in Algorithm 1.

3.3 Hyperbolic Operator in 2D: A Fully-Explicit Co-Located Scheme

We also present a preliminary 2D hyperbolic operator based on a fully-explicit co-located finite volume scheme. A monolithic solver is developed in this framework, considering, as done in 1D, the Rusanov fluxes for the spatial discretization of the convective terms and imposing the non-disturbance condition [1] for the non-conservative terms. On the other hand, for the divergence of the velocity in Eq. (1d), we use the Rhie and Chow interpolation of the velocity at cell interfaces to circumvent checker-boarding problems due to the low pressure-velocity coupling at low Mach number [14].

Algorithm 1 . Pseudo-code to solve the non-linear system resulting from the implicit time integration of the ODE system for pressure relaxation.

$\alpha_i^k \leftarrow \alpha_i^\diamond$, $\overline{P_{\mathrm{IN},i}} \leftarrow P_{\mathrm{IN}}^\diamond$, $\overline{e_i} \leftarrow P_i^\diamond$ ▷ Initialization
for $k = 0$ to $k_{\max}$ **do**
  $P_i^{k+1} \leftarrow$ solution of $f_P(P_i^{k+1}, \alpha_i^k)$ ▷ Solve Eq. (8)
  if $|P_1^{k+1} - P_2^{k+1}| < \epsilon$ **then**
    Exit loop ▷ $\mathbf{U}^{n+1} \leftarrow \mathbf{U}^{k+1}$
  else
    $\alpha_1^{k+1} \leftarrow \alpha_1^k - f(\alpha_1^k)/f'(\alpha_1^k)$ ▷ Solve Eq. (9)
    $\alpha_2^{k+1} \leftarrow 1 - \alpha_1^{k+1}$
    $\overline{e_i} \leftarrow \frac{1}{2}\left(e_i(\rho_i^k, P_i^{k+1}) + e_i^\diamond\right)$
    $\overline{P_{\mathrm{IN},i}} \leftarrow \frac{1}{2}\left(P_i^{k+1} + P_{\mathrm{IN}}^\diamond\right)$
  end if
end for

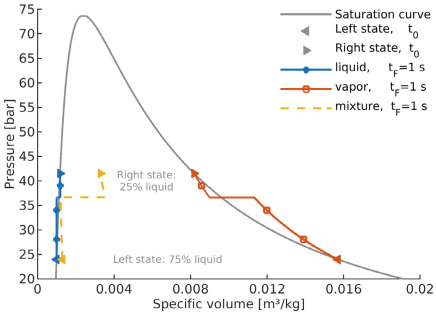

Fig. 1. Results of the CO_2 shock-tube test with instantaneous relaxation. The blue and the red lines show the states of the liquid and the vapor, respectively, within the whole domain. The yellow, dashed line shows the behavior of the mixture.

4 Results

The first test we present is a 1D shock-tube with instantaneous pressure and velocity relaxation, which means that mechanical equilibrium is imposed at each time step. The tube is filled with a liquid-gas mixture of CO_2 at saturated conditions. In the left chamber, the liquid volume fraction is $\alpha_{\mathrm{liq,L}} = 0.75$ and the temperature of both phase is $T_{\mathrm{L}} = 260$ K. In the right chamber, there is $\alpha_{\mathrm{liq,R}} = 0.25$ and $T_{\mathrm{R}} = 280$ K. The domain is 60 m long, and it is discretized with 600 uniform cells. The final time is $t_{\mathrm{f}} = 1$ s, reached in 2000 time steps. The results are shown in the $P - v$ plane in Fig. 1: each phase evolves close to "its side" of the VLE curve, governed by the Peng-Robinson EOS. On the other hand, if we look at the behavior of the mixture, whose density is defined as $\overline{\rho} = \alpha\rho_1 + \alpha\rho_2$, it evolves in the two-phase region, as expected. But, thanks to the modeling choice of having two pressures and two velocities, each phase can be described by its own EOS, without the need for an EOS for the mixture.

The second test is a preliminary assessment of the hyperbolic operator in 2D, and we do not consider any relaxation, so λ and μ are zero, and pressure and velocity disequilibrium can occur between phases. We present the simulation of the interaction of a shock-wave in air with a cylindrical bubble of helium. The domain is a rectangle ($[0, 300] \times [0, 47.5]$ mm) representing only half of the problem, thanks to the symmetry about the center-line, and it is discretized using an average grid spacing $\Delta x = 2$ mm and time step $\Delta t = 0.1$ μs. The initial flow field is separated into three regions: the cylindrical bubble, with a diameter of 5 mm, centered at $x_{\mathrm{B}}^0 = 196$ mm and characterized by $\alpha_{\mathrm{He}} = 0.93$, the left and the right regions separated by the shock-wave located at $x_{\mathrm{s}}^0 = 235$ mm with $\alpha_{\mathrm{air}} = 0.93$. The left and the bubble regions are initialized with the pre-shock pressure $P_{\mathrm{L}}^0 = 10^5$ Pa and density $\rho_{\mathrm{L,air}}^0 = 1.4$ kg/m^3; the right region is initialized with the post-shock state corresponding to a shock Mach number in

air of $M_s = 1.22$. For helium, a uniform initial density $\rho^0_{He} = 0.2546$ kg/m^3 is imposed everywhere. The final simulation time is $t_f = 900\mu$s, reached in 9000 time steps.

Figure 2 shows the flow field at different times, before, during, and after the shock-bubble interaction. The bubble deformation is qualitatively in agreement with the numerical data by Daude et al. [5] and experimental results by Hass and Sturtevant [6]. This can be better appreciated in Fig. 3, where the bubble interface obtained with the proposed method is superimposed on the experimental results. More specifically, the background picture is the shadow photograph taken from Fig. 7(h) in [6], 427 μs and 674 μs after the shock-bubble interaction, and the violet lines represent the contour lines $\alpha_{He} = 0.3$ and $\alpha_{He} = 0.7$ at the same time. A good agreement shows the validity of the proposed approach.

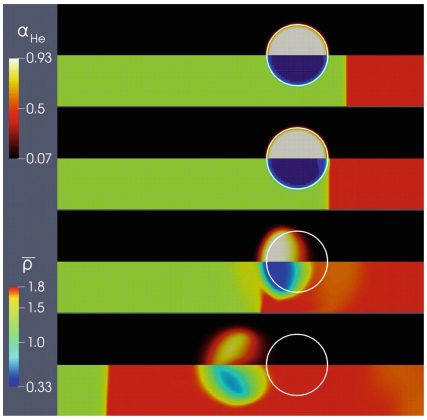

Fig. 2. Shock and air/He bubble interaction. Contour plots of helium volume fraction α_{He} (upper part) and mixture density $\overline{\rho}$ (bottom part), at different times. The white circle displays the initial position of the bubble.

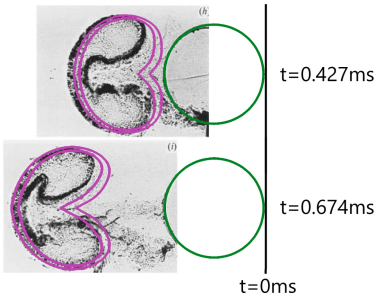

Fig. 3. Shock and air/He bubble interaction. Comparison of the position and shape of the bubble between experiment data from [6] (background picture) and the numerical data (violet isolines at $\alpha_{He} = \{0.3, 0.7\}$, 427 μs and 674 μs after the shock-bubble interaction, i.e., at the simulation times $t = 467$ μs and $t = 714$ μs. The green circles display the initial positions of the bubble.

5 Conclusions and Future Works

We presented a solution strategy for a pressure-based Baer-Nunziato-type model for compressible two-phase flows. The rejection of the assumption of thermo-mechanical equilibrium allows the description of each phase with its own thermodynamic model, which could consist of any generic pressure EOS in the form

$e = e(P, \rho)$ and the compatible caloric EOS. Two numerical methods were tested: a semi-implicit finite-volume scheme over staggered grids in 1D, and a co-located explicit finite-volume scheme in 2D. The former one was equipped with instantaneous pressure and velocity relaxation, and it showed the possibility to simulate flow problems where the two-phase mixture evolves within the VLE curve, without the need to define a mixture EOS. The latter has been the first step toward an all-Mach monolithic 2D numerical method for the simulation of two-phase flows over unstructured grids. The preliminary implementation of the explicit hyperbolic solver has been validated through the simulation of the interaction between a shock wave in air and a bubble of helium.

The current and future developments follow two main paths: the BN-type model will be equipped with new relaxation terms to include mass and heat transfer, and the implementations of the numerical scheme will be improved by including higher order discretization and the source operator also in 2D.

Acknowledgements. R.A. is partially funded by SNF Grant 200020_204917. G. S. was partialy funded by R.A's UZH Einrichtungkredit.

References

1. Abgrall, R.: How to prevent pressure oscillations in multicomponent flow calculations: a quasi conservative approach. J. Comput. Phys. **125**(1), 150–160 (1996). https://doi.org/10.1006/JCPH.1996.0085
2. Baer, M.R., Nunziato, J.W.: A two-phase mixture theory for the deflagration-to-detonation transition (DDT) in reactive granular materials. Int. J. Multiphase Flow **6**, 861–889 (1986). https://doi.org/10.1016/0301-9322(86)90033-9
3. Brown, S., Martynov, S., Mahgerefteh, H., Chen, S., Zhang, Y.: Modelling the non-equilibrium two-phase flow during depressurisation of CO_2 pipelines. Int. J. Greenhouse Gas Control. **30**, 9–18 (2014). https://doi.org/10.1016/j.ijggc.2014.08.013
4. Brown, S., Martynov, S., Mahgerefteh, H., Proust, C.: A homogeneous relaxation flow model for the full bore rupture of dense phase CO_2 pipelines. Int. J. Greenhouse Gas Control. **17**, 349–356 (2013). https://doi.org/10.1016/j.ijggc.2013.05.020
5. Daude, F., Galon, P.: On the computation of the Baer-Nunziato model using ALE formulation with HLL- and HLLC-type solvers towards fluid-structure interactions. J. Comput. Phys. **304**, 189–230 (2016). https://doi.org/10.1016/j.jcp.2015.09.056
6. Haas, J.-F., Sturtevant, B.: Interaction of weak shock waves with cylindrical and spherical gas inhomogeneities. J. Fluid Mech. **181**, 41 (1987). https://doi.org/10.1017/S0022112087002003
7. Métayer, O.L., Saurel, R.: The Noble-Abel Stiffened-Gas equation of state. Phys. Fluids. **28**, 046102 (2016). https://doi.org/10.1063/1.4945981
8. Re, B., Abgrall, R.: Numerical simulation of weakly compressible multiphase flows with a Baer-Nunziato type model. World Congr. Comput. Mech. ECCOMAS Congr. **600**, 1–12 (2021). https://doi.org/10.23967/wccm-eccomas.2020.247
9. Re, B., Abgrall, R.: A pressure-based method for weakly compressible two-phase flows under a Baer-Nunziato type model with generic equations of state and pressure and velocity disequilibrium. Int. J. Numer. Meth. Fluids **94**(8), 1183–1232 (2022). https://doi.org/10.1002/fld.5087

10. Re, B., Guardone, A.: An adaptive ALE scheme for non-ideal compressible fluid dynamics over dynamic unstructured meshes. Shock Waves **29**, 73–99 (2019). https://doi.org/10.1007/s00193-018-0840-2
11. Saurel, R., Abgrall, R.: A multiphase Godunov method for compressible multifluid and multiphase flows. J. Comput. Phys. **150**(2), 425–467 (1999). https://doi.org/10.1006/JCPH.1999.6187
12. Saurel, R., Pantano, C.: Diffuse-interface capturing methods for compressible two-phase flows. Annu. Rev. Fluid Mech. **50**, 105–130 (2018). https://doi.org/10.1146/annurev-fluid-122316-10.1146/annurev-fluid-122316-050109
13. Saurel, R., Petitpas, F., Berry, R.A.: Simple and efficient relaxation methods for interfaces separating compressible fluids, cavitating flows and shocks in multiphase mixtures. J. Comput. Phys. **228**, 1678–1712 (2009). https://doi.org/10.1016/j.jcp.2008.11.002
14. Sirianni, G., Re, B., Abgrall, R., Guardone, A.: Momentum weighted interpolation for unsteady weakly compressible two-phase flows on unstructured meshes. J. Comput. Appl. Math. **428**, 115209 (2023). https://doi.org/10.1016/j.cam.2023.115209
15. White, M.T.: Cycle and turbine optimisation for an ORC operating with two-phase expansion. Appl. Thermal Eng. **192**, 116852 (2021). https://doi.org/10.1016/j.applthermaleng.2021.116852
16. Wilhelmsen, Ø., et al.: Thermodynamic modeling with equations of state: present challenges with established methods. Indus. Eng. Chem. Res. **56**, 3503–3515 (2017). https://doi.org/10.1021/acs.iecr.7b00317